

SIMULATIONS OF LASER FIELD EMISSION FROM NANOSTRUCTURES WITH IMAGE CHARGE TRAPPING AND BAND STRUCTURE TRANSITIONS*

B. Wang[†], G. E. Lawler, J. I. Mann, J. B. Rosenzweig, UCLA, Los Angeles, CA 90024, USA
S. Karkare, Arizona State University, Tempe, AZ 85287, USA
J. K. Nangoi, T. Arias, Cornell University, Ithaca, NY 14850, USA

Abstract

Laser-induced field emission from nanostructures as a means to create high brightness electron beams has been a continually growing topic of study. Experiments using nanoblade emitters have achieved peak fields upwards of 40 GV/m, begging further investigation in this extreme regime. A recent paper has provided analytical reductions of the common semi-infinite Jellium system for pulsed incident lasers. We utilize these results as well as similar previous results to further understand the physics underlying electron rescattering-type emissions. We progress in numerically evaluating the analytical solution to attempt to more efficiently generate spectra for this system. Additionally, we use the full 1-D time-dependent Schrödinger equation with a Hartree potential and a dispersion-relation transition from material to vacuum to study the same system. We determine what importance the inclusion of the material band structure may have on emissions using this computationally challenging approach.

INTRODUCTION

The bright, coherent electron beams that can be generated from nanoscale emitters have proven to be useful for such applications as electron microscopes [1], electron interferometry, nanometric imaging, synchrotrons [2], and more. A popular choice of nanostructure for electron emission, the nanotip, suffers from material breakdown when subjected to peak surface fields on the order of 10 GV/m [3, 4]. This problem of material breakdown is mitigated by the usage of a similar nanostructure, the nanoblade, which is essentially an extruded nanotip. Due to its improved thermomechanical properties, the nanoblade can survive peak surface fields over 40 GV/m and potentially even up to 80 GV/m [5, 6], allowing for higher current densities.

To investigate electron emission from nanoblades, we solve the 1-D time-dependent Schrödinger equation (TDSE), making use of recently published analytical solutions. We also perform finite difference numerical simulations investigating the effects that a collective image potential and the material's effective mass have on yields.

* This research is supported by the Center for Bright Beams, U.S. National Science Foundation grant PHY-1549132.

[†] benjaminwang1@g.ucla.edu

ANALYTICAL SOLUTION FROM REF. [7]

We use the analytical solution [7] to the TDSE,

$$i\partial_t\psi(x,t) = -\frac{1}{2}\Delta\psi(x,t) + \Theta(x)(U - Ex\cos(\omega t))\psi(x,t) \quad (1)$$

derived in Ref. [7] with the laser energy $\omega = 1.55 \text{ eV} = 0.0570$ atomic units (a.u.), total metallic potential depth $U = 10 \text{ eV} = 0.3676$ a.u., and Fermi energy $E_f = 4.5 \text{ eV} = 0.165$ a.u. to represent a gold cathode under the illumination of an 800 nm laser. In this model, the uniform cosine laser field is turned on instantaneously at $t = 0$.

The resulting yield curves exhibit the expected fourth power yield to laser intensity scaling for four-photon emission. The deviation from this power law at higher laser intensities is indicative of channel closing [8]. These features are corroborated by Fig. 4 in Ref. [9].

The difficulties that we encountered were related to computational complexity, as the required computation time increased dramatically with the temporal boundary and the electric field magnitude, which made calculations for longer periods and/or higher fields take much longer than numerical simulation. This difficulty was compounded by the fact that, in Eq. (1), there is a discontinuity caused by the instantaneous application of the cosine field at $t = 0$, which makes the results from the first few periods largely nonphysical. The termination time then needs to be somewhat large to find the asymptotic current. Reference [10] covers these findings in more detail.

ANALYTICAL SOLUTION FROM REF. [11]

A more recent paper [11] analytically solves the TDSE for periodic Gaussian pulses, so that the applied laser field is of the form,

$$F(t) = F_0 + F_1 e^{-t^2/\sigma^2} \cos(\omega t + \phi) \quad (2)$$

which resolves the discontinuity difficulty of Eq. (1). We use same parameters as before as well as static field $F_0 = 0$, carrier envelope phase (CEP) $\phi = \frac{\pi}{2}$, full-width at half-maximum (FWHM) power $\tau_p = \frac{10\pi}{\omega}$ (5 periods), and $m = 20$ cycles between pulses. Again the yield curve exhibits the expected fourth power yield to laser intensity scaling for four-photon emission, however we experience numerical issues at higher fields starting at around $F_1 = 10 \text{ V/nm}$, as can be seen in the yield curve in Fig. 1. For channel closing to be the culprit, we would expect to find a periodic drop in

Content from this work may be used under the terms of the CC BY 4.0 licence (© 2022). Any distribution of this work must maintain attribution to the author(s), title of the work, publisher, and DOI

yield as each photon channel closes in succession with the rising ponderomotive potential; this is not observed.

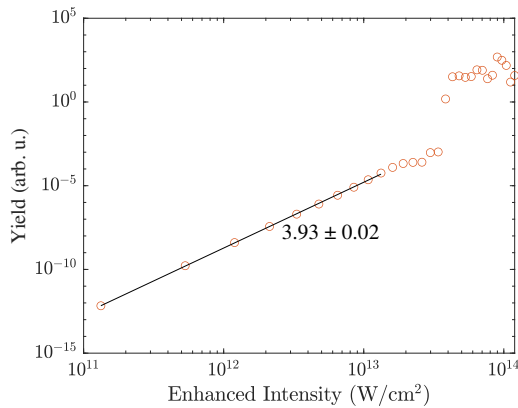


Figure 1: Yield curve for 800 nm laser field emission from gold for a Gaussian pulse with a FWHM of 5 periods. The fourth power yield to laser intensity scaling is expected for the four photon emission regime, but the data becomes unreliable beyond an intensity of about 10^{13} W/cm² due to numerical issues at higher fields.

These numerical issues at higher fields are also apparent in the graphs of transmission probability versus emitted electron energy (which is related to the emission spectrum). These pseudo-spectra are shown in Fig. 2. These graphs have oscillations that become noisier the higher the electric field magnitude, as can be seen by the jagged appearance of the 20 V/nm spectrum as compared to the much smoother 1 V/nm spectrum. The appearance of this apparent noise is unaffected by increasing the number of integration steps, so the noise is likely caused not by computational constraints, but by other factors. One such factor under consideration is interference between the emissions of temporally adjacent pulses.

We also note that the 20 V/nm spectrum does not extend as far out in energy as expected. According to the semi-classical cutoff of $10U_p$ we would expect emission energies out to about 30 eV.

While the channels with negative energy in vacuum do not contribute to the yield, we include them in Fig. 2 as a demonstration of our current issues.

IMAGE CHARGE LIMITED YIELD

We revisit some of the simulations discussed in Ref. [5] where we found a nearly linear yield and intensity relation at high fields, which is consistent with the collective image potential trapping model. We noted that the yield would likely be dependent on the simulation size and that, using a proper Hartree potential model, the results should converge to the observed linear scaling provided an infinitely large simulation.

Figure 3 shows yield curves in the space-charge limited regime with simulated vacuum lengths varying from 800 Å to 2000 Å. We find that, as we increase the vacuum length

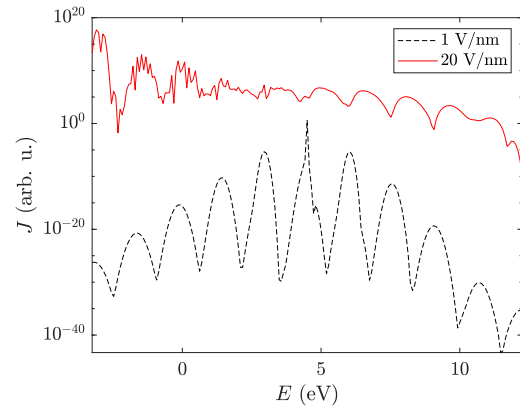


Figure 2: Transmission probability versus emitted electron energy for 800 nm laser field emission from gold for a Gaussian pulse with a FWHM of 5 periods. The oscillations in these graphs are apparent for higher electric field magnitudes, indicating possible numerical or modeling issues.

of the simulation, the power law decreases below the expected linear scaling at these fields. At 2000 Å we even see a decreasing yield for increasing laser intensities.

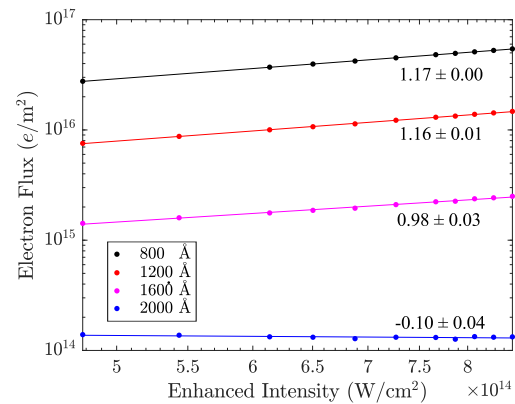


Figure 3: Yield curves in the space-charge limited regime with simulation lengths in vacuum of 800 Å (black), 1200 Å (red), 1600 Å (magenta), and 2000 Å (blue). The power law exponents fitted to the data are adjacent to their respective curves. We observe that, with increasing simulation length, the power law diminishes to below the expected linear scaling.

We believe this nonphysical behavior arises due to the absorptive boundary on the material side of the simulation. As the electron rescattering process progresses, some wavefunction transmits through the Jellium slab and reaches the back end of the simulation where it is absorbed by an imaginary potential. The total charge within the simulated slab is now diminished not only by the electrons which emit from the system into vacuum, but also by those which would nominally continue to exist within the material.

Based on the cylindrical geometry used in the model, the absorption of these electrons is not inhibited by the buildup of positive charge in the outer “shell” which makes up the

Jellium slab. Thus, with increasing laser intensity this charge buildup can only increase. The electrons in vacuum, however, observe this increase in positive charge and are therefore attracted back to the cathode. With larger simulation sizes these electrons have a larger potential to climb and therefore are more likely to be reabsorbed, reducing the total yield.

INCLUSION OF EFFECTIVE MASS

It is known that the dispersion relation for an electron in transport may be simply modeled using an effective mass within the material for applications in photoemission [12]. To model a material like gold we use an effective mass of $m_{eff} = 1.1$ within the material and the standard electron mass in vacuum. The transition between the two regimes is modeled by a spatially variable kinetic energy operator,

$$T(x) = \frac{1}{2m_e} \hat{p} \left(\frac{1}{m_{eff}} (1 - S(x)) + S(x) \right) \hat{p} \quad (3)$$

with $S(x) = \frac{1}{1+e^{-\kappa x}}$ a sigmoid function. We use the transition rate $\kappa = 1 \text{ nm}^{-1}$, which is a relatively smooth transition compared to the Jellium potential [5].

Continuing the simulation methods in Ref. [5], the inclusion of a spatially-dependent dispersion relation is not straightforward using the operator-splitting Fourier method as the kinetic operator is no longer spatially invariable. We work around this by expanding the unitary kinetic half-propagator, which follows Strang splitting of the full propagator, into a fourth order Taylor series,

$$e^{-\frac{i}{2\hbar} T dt} \approx \sum_{n=0}^4 \frac{(-\frac{i}{2\hbar} dt T)^n}{n!} \quad (4)$$

We Fourier transform back and forth to apply the momentum-space and real-space operators. The simulation initialization is done such that the charge density within the slab remains the same, according to the Fermi energy of gold. We do not include any Hartree or collective image potential and the laser pulse FWHM power is increased to 35 fs.

A yield curve comparing the yields from the gold effective mass calculation to one which uses the standard electron mass throughout is shown in Fig. 4. For intensities greater than $3 \times 10^{13} \text{ W/cm}^2$ we observe a relatively nontrivial dependence on the field intensity. For the data accrued the average ratio of yields is 0.96, however the actual ratio at any given field strength is variable by an order of about 0.1. Otherwise, this appears to be a relatively minute correction for the yield curves. A stronger effect might be seen for other materials or for other quantities such as the mean transverse energy (MTE), which are currently under consideration.

For lower incident intensities we find that the yields in the calculation utilizing the effective mass boundary are increased. We attribute this to numerical error, as a calculation we performed with zero field strength also resulted in a comparable yield. Mitigation of this error takes two forms. We

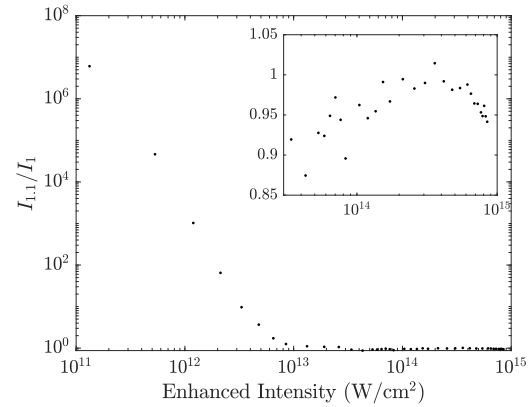


Figure 4: Ratio of yields for calculations using an effective mass of $1.1m_e$ within the Jellium slab to those for an effective mass of $1m_e$ throughout. The inset shows the same data for intensities greater than $3 \times 10^{13} \text{ W/cm}^2$ and with a linear y-axis scaling.

may either decrease the temporal or spatial step sizes, which increases computation time (which is already on the order of weeks). We may also decrease the transition rate, which alters our physical model. Neither are optimal approaches.

CONCLUSION

The prospect of using the analytical solution derived in Ref. [11] to solve the 1-D TDSE is promising for multiple reasons. Firstly, this solution is computationally efficient to evaluate, with a yield curve calculation on the scale of Fig. 1 taking around half an hour to run on a laptop. This contrasts previous efforts Ref. [10] where calculations could take weeks on a more powerful server computer. Secondly, this solution offers many customizable parameters that allow us to adjust and investigate properties such as the pulse length, bias field, and CEP. Finally, this solution straightforwardly calculates the full wave function itself, which we may use to calculate a true spectrum [13]. This will allow us to factor in space-charge trapping in a computationally efficient manner.

Our work involving the collective image potential is still ongoing. We found that a simulation parameter, the vacuum length, strongly affects the resulting observed behavior. A model which either does not absorb charge on the inner boundary or assumes a perfect conductor for a strictly image potential-based system are likely our next approaches.

We find that the inclusion of the effective mass in TDSE-based simulation is relatively unimportant for materials where $m_{eff} \approx 1$. Most of the deviations we find arise from numerical issues involving the inclusion of a spatially variable kinetic operator. Analytical corrections to the transmission and reflection coefficients of the surface barrier may provide better insight to the relevance of this property.

REFERENCES

- [1] C. Ropers, D. R. Solli, C. P. Schulz, C. Lienau, and T. Elsaesser, "Localized multiphoton emission of femtosecond

- electron pulses from metal nanotips,” *Phys. Rev. Lett.*, vol. 98, p. 043 907, 4 Jan. 2007.
- [2] P. Hommelhoff, Y. Sortais, A. Aghajani-Talesh, and M. A. Kasevich, “Field emission tip as a nanometer source of free electron femtosecond pulses,” *Phys. Rev. Lett.*, vol. 96, p. 077 401, 7 Feb. 2006.
- [3] M. Krüger, C. Lemell, G. Wachter, J. Burgdörfer, and P. Hommelhoff, “Attosecond physics phenomena at nanometric tips,” *Journal of Physics B: Atomic, Molecular and Optical Physics*, vol. 51, no. 17, p. 172 001, Aug. 2018.
- [4] R. Bormann, M. Gulde, A. Weismann, S. V. Yalunin, and C. Ropers, “Tip-enhanced strong-field photoemission,” *Phys. Rev. Lett.*, vol. 105, p. 147 601, 14 Sep. 2010.
- [5] J. I. Mann, T. Arias, G. E. Lawler, J. K. Nangoi, and J. B. Rosenzweig, “Simulations of Nanoblade-Enhanced Laser-Induced Cathode Emissions and Analyses of Yield, MTE, and Brightness,” in *Proc. IPAC’21*, Campinas, Brazil, May 2021, pp. 2957–2960. doi:10.18429/JACoW-IPAC2021-WEPAB147
- [6] G. E. Lawler, J. I. Mann, J. B. Rosenzweig, R. J. Roussel, and V. S. Yu, “Initial Nanoblade-Enhanced Laser-Induced Cathode Emission Measurements,” in *Proc. IPAC’21*, Campinas, Brazil, May 2021, pp. 2814–2817. doi:10.18429/JACoW-IPAC2021-WEPAB097
- [7] O. Costin, R. Costin, I. Jauslin, and J. L. Lebowitz, “Exact solution of the 1d time-dependent schrödinger equation for the emission of quasi-free electrons from a flat metal surface by a laser,” *Journal of Physics A: Mathematical and Theoretical*, vol. 53, no. 36, p. 365 201, Aug. 2020.
- [8] R. Kopold, W. Becker, M. Kleber, and G. G. Paulus, “Channel-closing effects in high-order above-threshold ionization and high-order harmonic generation,” *Journal of Physics B: Atomic, Molecular and Optical Physics*, vol. 35, no. 2, pp. 217–232, Jan. 2002.
- [9] S. Yalunin, M. Gulde, and C. Ropers, “Strong-field photoemission from surfaces: Theoretical approaches,” *Phys. Rev. B*, vol. 84, Nov. 2011.
- [10] B. Wang, J. I. Mann, and J. B. Rosenzweig, “Analytical solution of the 1d tdse for strong laser field electron emission,” *UCLA USJ*, 2022.
- [11] Y. Luo, Y. Zhou, and P. Zhang, “Few-cycle optical-field-induced photoemission from biased surfaces: An exact quantum theory,” *Phys. Rev. B*, vol. 103, p. 085 410, 8 Feb. 2021.
- [12] S. Karkare *et al.*, “Monte carlo charge transport and photoemission from negative electron affinity gaas photocathodes,” *Journal of Applied Physics*, vol. 113, no. 10, p. 104 904, 2013.
- [13] J. Mann and J. Rosenzweig, *A coherent bi-directional virtual detector for the 1-d schrödinger equation*, 2022. doi:10.48550/ARXIV.2205.10461